Climate Dynamics (2020) 55:909–923
https://doi.org/10.1007/s00382-020-05300-8

Internal variability and external forcings in the ocean–atmosphere multidecadal oscillator over the North Atlantic

Pedro Ribera[1] · **Paulina Ordoñez**[2] · **David Gallego**[1] · **Cristina Peña-Ortiz**[1]

Received: 15 June 2019 / Accepted: 18 May 2020 / Published online: 23 May 2020
© Springer-Verlag GmbH Germany, part of Springer Nature 2020

Abstract
In this paper, we generalize the concept of "external forcing" to include any mechanism that modulates the long-term evolution of a meteorological variable but is not directly related to the internal variability of the climate system. Applying this concept, the corresponding 'external forcings' are removed from several long record datasets of oceanic and atmospheric variables at the surface in the North Atlantic. We perform a multivariate analysis in the frequency domain over both the original data fields and the new 'internal variability' fields. This multivariate analysis is based on a MultiTaper Method-Singular Value Decomposition (MTM-SVD). It is noteworthy that, after the removal of the external forcings, there is an almost perfect alignment of the main multidecadal oscillatory band (f = 0.21 cycles/decade) with all the spectra of the analysed fields. This alignment was not observed before the external forcings were removed. Particularly striking is the case of the sea level pressure (SLP), which shows a notable variation in its oscillation period despite the fact that this variable has traditionally been considered to be unaffected, at global scale, by any external forcing. The external forcing in the SLP records is very probably caused by the scarcity of the observed data during the first hundred years of the record (most evident, during the earliest decades), by the spatial distribution of those observations and, possibly, by the assimilation model employed to build those long record datasets. When we analysed the relationship between the ocean and the atmosphere using this approach, we found strong evidence of a cyclic behaviour in which oceanic conditions modulate the atmospheric variability, with a lead time of up to about 10 years.

Keywords Atlantic multidecadal oscillation (AMO) · SST reanalyses · Twentieth century reanalysis · Internal climate variability · Blockings · NAO · MTM-SVD · External forcings

1 Introduction

In the mid-1980s, early publications about a coherent multidecadal oscillation in various climatic variables at the sea surface appeared in the scientific literature (e.g. Folland et al. 1984, 1986). In subsequent years, several papers were published which described multidecadal oscillations, with periods ranging from 40 to 70 years, mostly centred over the North Atlantic sector but with global implications (e.g. Schlesinger and Ramankutty 1994; Mann et al. 1995; Delworth and Mann 2000, etc.). There was an apparent consensus about the existence of a cold period (1920s)—warm period (1940–1950s)—cold period (1970–1980s) sequence over the North Atlantic through the twentieth century (Folland et al. 1986; Deser and Blackmon 1993; Kushnir 1994). The problem was that it was difficult to confidently define such a multidecadal oscillatory signal with about a century of observed data. Later studies extended the analysis back to the mid-nineteenth century using the Kaplan et al. (1998) sea surface temperature (SST) reanalysis, identifying an oscillation with a period of 50–60 years (Tourre et al. 1999; Delworth and Mann 2000). A few years later, Kerr (2000) presented a general description of a multidecadal oscillation over the North Atlantic and, we believe, used the term 'Atlantic multidecadal oscillation' (AMO) for the first time. AMO has become the usual term for any climatic oscillation centred in the North Atlantic basin and having a characteristic period longer than two decades. Periods of between 40 and 70 years are the most common.

✉ Pedro Ribera
pribrod@upo.es

[1] Departamento de Sistemas Físicos, Químicos y Naturales, Universidad Pablo de Olavide, 41013 Seville, Spain

[2] Centro de Ciencias de la Atmósfera, Universidad Nacional Autónoma de México, 04510 Mexico City, Mexico

These multidecadal oscillations are thought to be genuine quasiperiodic cycles of internal climate variability, although the mechanisms implied in these oscillations remain controversial. Knight et al. (2005) found that models had to include deep ocean circulation to spontaneously produce multidecadal oscillations. In recent years, the Atlantic thermohaline circulation, involving the variability of the Atlantic Meridional Overturning Circulation (AMOC) has been proposed as one of the mechanisms capable of explaining such long-lasting oscillations (e.g. Knight et al. 2005; Ting et al. 2009). As well, some models have shown that different feedback processes involving the atmosphere, the oceans, particularly the Atlantic Ocean, and ice cover are somehow involved in the existence of the different oscillatory periods (Dijkstra et al. 2014; Jamet et al. 2016; among others). Frankcombe et al. (2010) suggested that the origin of the 45–70-year oscillation could be associated with a coupling between Atlantic and Arctic circulations, or with a slow deep circulation in the Atlantic. Some authors have proposed that atmospheric patterns like the presence and persistence of blockings over the northern North Atlantic or a persistence of the North Atlantic Oscillation (NAO) in one of its phases could be important for the evolution and phase transition of the AMO (Häkkinen et al. 2011; Li et al. 2013; McCarthy et al. 2015; Hanna et al. 2016; Jamet et al. 2016). Conversely, other authors suggest that it is the ocean and its associated variability that induces changes in atmospheric circulation patterns, favouring the persistence of a particular phase of the NAO or modulating the frequency of blockings over the area (Gulev et al. 2013; Peings and Magnusdottir 2014; Wills et al. 2019). Of course, the two approaches are not mutually exclusive.

This controversy comes in part from the difficulties in separating internal from external variability in climatic data. Those forcings caused by mechanisms which are not part of the internal dynamics of the climatic system will be termed 'external forcings' throughout this paper. External forcings include externally imposed radiative forcings, like those caused by human emissions of greenhouse gasses or by volcanic aerosol emissions; but external forcings also include possible non-climatic errors in the data. In most of the early papers in which AMO-like oscillations were described, linear detrending was applied to the data to remove long term external forcings. However, in the last decade, more recent publications have suggested that the application of linear detrending is probably not the appropriate method to eliminate those external forcings, and that it could somehow distort the results (Trenberth and Shea 2006; Ting et al. 2009; Mann et al. 2014; Wills et al. 2019). Some of those papers showed that a direct application of linear detrending modified the period, phase and/or amplitude of the resulting multidecadal oscillations, so that some of the impacts attributed to the AMO changed depending on how external forcings were removed. For example, the AMO showed a noticeable impact on Atlantic hurricane activity that almost disappeared when the radiative forcing caused by greenhouse gases or volcanic emissions was separated from the actual AMO signal (Mann and Emanuel 2006). Results obtained from different model runs under different emissions scenarios reinforce this idea about the importance of separating the internal AMO signal from any external forcing if AMO is to be adequately characterized as an internal mode of climatic variability (Frankcombe et al. 2015).

Another key point that has made it difficult to reliably identify multidecadal climate signals is the restricted duration and spatial coverage of instrumental climate data. We attempt to deal with these limitations by using the longest available reanalyses for SST and atmospheric variables. All these reanalyses are generated by assimilating observational data with a climate model that generates series of the variable of interest at every point of a regular grid and at regular time steps. In this sense, the model 'creates' series based on the information from instrumental observations in the nearby area, but none of those gridded series can be regarded as direct observations. The time coverage of the observational data in these datasets extends from the mid-nineteenth century to the present, covering between two and three complete cycles of a 40–70 years oscillatory signal, as described in the next section. Finally, a robust and well-proven signal detection method is applied to these datasets, before and after external forcings are removed, to detect the multidecadal oscillatory signal contained within them.

This paper has a threefold aim. First, we perform an updated comparison among several datasets in order to assess the coherence and robustness of the multidecadal oscillatory signals contained within them, with a special focus on the coherence between atmospheric and oceanic oscillations. Second, we adopt the generalized definition of external forcings to separate internal and external components of the variability to better understand the physical mechanism involved in the coupling between the ocean and the atmosphere over the North Atlantic, as well as between surface pressure and temperature in the atmosphere. We discuss the main characteristics of those 'internal' oscillations and some of the physical mechanisms involved as well. Finally, we make use of the new results to try to shed new light on the ongoing debate about whether it is the ocean that induces changes in the atmospheric circulation patterns at multidecadal scales or vice versa.

Section 2 of this paper includes a description of the data plus a description of the methodology used to identify and characterize multidecadal oscillations. Section 3 describes the results obtained with the different datasets and compares our findings with results reported previously in the literature. Section 4 includes a discussion of the results and highlights our main conclusions.

2 Data and methods

2.1 Reanalyzed datasets

Four SST datasets have been analysed with the aim of identifying and characterizing multidecadal oscillations within the North Atlantic basin. The four datasets are Kaplan extended SST v2, COBE SST v2, NOAA-Extended Reconstructed SST v3b and Hadley SST dataset, henceforth identified as Kaplan, COBE, ER and Hadley. These datasets are freely accessible online from the Earth System Research Laboratory and all of them include monthly SST gridded data starting in the mid-nineteenth century. In general, data included in these datasets are considered quite reliable over the last six or seven decades, and the authors consider the quality of the data to be adequate over several regions of the world, particularly over the Atlantic Ocean, for the whole available period.

The ER dataset uses the International Comprehensive Ocean and Atmosphere Data Set (ICOADS: Woodruff et al. 1998; Woodruff et al. 2011) as its main source of observed data. The spatial resolution of ER SST is 2° latitude × 2° longitude, and it covers the period from 1854 to the present. Several authors explain that for the North Atlantic sector, this reanalysis is of the highest quality before 1880 (Xue et al. 2003; Smith and Reynolds 2003, 2004a; Smith et al. 2008). Like any of the other SST reanalyses, updated versions of ER-SST, which are published every few years, include successive improvements in data quality. For example, the ER-SST v3b data for the late nineteenth century is said to be noticeably improved over version v2, obtained by an 'improved tuning of the analysis methods' (Smith et al. 2008). In general, the NOAA ESRL-PSD website, where these reanalyses are available, includes a short description of the successive modifications included in each version of each of these reanalyses.

The Kaplan dataset consists of monthly anomalies, with coverage from 1856 to the present. Its spatial resolution is 5° latitude × 5° longitude. It uses the Meteorological Office Historical Sea Surface Temperature data set (Parker et al. 1994) version of the Global Ocean Surface Temperature Atlas data set from the UK. MET Office as the input for the SST data. Kaplan also incorporates data from ICOADS to fill gaps when and where no other data is available. In the original publication in which this reanalysis was presented for the first time, it was explained that monthly SST anomalies were produced using three statistically based methods: optimal smoothing, the Kalman filter and optimal interpolation. Of course, these methods had to be accompanied by other methods able to estimate errors in the analysed fields. A complete description of how this reanalysis was carried out can be found in Kaplan et al. (1998).

The COBE dataset is the longest, starting in 1850. Its spatial resolution is 1° latitude × 1° longitude. It incorporates ICOADS data (like the ER dataset) and a set of extra SST observations around Japan before World War II. In addition, it includes some additional observational datasets, but mainly for recent periods. In recent versions of this reanalysis, physical mechanisms, such as the relationship between ice and SST, are employed to improve the quality of the SST dataset. As well, several advanced statistical methods are used to reduce biases in the pre-analysis period or those caused over data-sparse regions. These methods are described in detail in Ishii et al. (2005) and Hirahara et al. (2014).

Finally, the source data for the Hadley dataset is the Met Office Marine Data Bank (MDB), but it relies on ICOADS data where no MDB data is available. This dataset includes observations from 1870 to the present, with a 1° latitude × 1° longitude spatial resolution. As with the previous reanalyses, the Met Office webpage (https://www.metoffice.gov.uk/hadobs/hadisst/) includes some insights about how the dataset was generated: 'temperatures are reconstructed using a two-stage reduced-space optimal interpolation procedure, followed by superposition of quality-improved gridded observations onto the reconstructions to restore local detail'. A very detailed description of this reanalysis can be found in Rayner et al. (2003).

ICOADS is, therefore, a common source of data for all these datasets. However, as the authors of the different datasets recognize, there are differences among them, particularly before 1880. Some of these differences are due to the use of different assimilation models. But the use of additional or alternative datasets is thought to be the main cause of these differences, especially for the nineteenth century when observations were scarcer. Differences in data bias adjustments are responsible for many of the discrepancies before roughly 1950.

In order to characterize the atmospheric branch of multidecadal-scale variability, data from the twentieth century Reanalysis v2c (20CR; Compo et al. 2006; Compo et al. 2011) has been used. This reanalysis is based on surface observations of synoptic pressure, monthly sea surface temperature and sea ice distribution. We have used monthly mean values of mean sea level pressure (SLP); and air temperature, zonal wind and meridional wind at sigma level 0.995 (T, u and v) over the period 1851–2014.

Finally, and in order to validate some of the spectral characteristics obtained from the 20CR data, air temperature at the surface (T2m) and SLP from the ERA twentieth century reanalysis (ERA20C: Poli et al. 2016) were used. Temporal and spatial resolutions employed with these data are coincident with those of the 20CR, but ERA20C has a shorter length, beginning the monthly series in 1900 and ending in 2010.

Subsets from all of these databases were extracted and prepared as follows. We considered the region between 0°N and 80°N, and from 80° W to 0° E. A 2° latitude × 2° longitude resolution has been adopted for all the datasets except Kaplan, which had an original resolution of 5° latitude × 5° longitude. The spatial resolution of the wind fields was reduced to a 4° × 4° grid. All of the series except Hadley start in January 1856 (Hadley in January 1870) and they continue until December 2016 (with the exception of 20CR, which ends in December 2014). All of the series have been converted into annual anomalies by subtracting the long-term monthly values from the corresponding monthly series and then averaging the corresponding monthly anomalies for each year.

2.2 Internal variability vs. external forcings

As was noted in the introductory section, it is critical to remove any externally forced signal contained in the observational or modelled data in order to identify the actual internal climate signal (see, for example, Frankcombe et al. 2015). Thus, once all our original series were converted into annual anomalies, the externally forced signal and the internal variability were separated for each grid point and variable following the method described in Ting et al. (2009). In their approach, the evolution of the global mean value of the selected variable is used as a proxy for the externally forced signal. Then, each two-dimensional field is regressed on the time series of the corresponding globally averaged variable. An estimate of the local internal component of the climatic signal is then obtained as the difference between each grid point in the original series and its corresponding regression coefficient. The evolution of the global mean values of the different variables was computed as the area weighted mean value between 60° S and 60° N for SST, as suggested by Ting et al. (2009), and between 85° S and 85° N for the atmospheric variables (see Fig. 1 for examples of evolution of global air temperature and SLP anomalies).

There are notable differences in the nature of the external forcings between variables measuring surface temperature (both oceanic and atmospheric) and any other variable, particularly SLP. The observed evolution of global surface temperature (Fig. 1a) is mainly affected by the anthropogenic emission of greenhouse gases (GHG) showing periods of accelerated heating with otherwise a slower rise in temperature or even a slight cooling. By contrast, we would have expected the global mean value of SLP to remain approximately constant since the total mass of the atmosphere is constant. However, Fig. 1b shows that it has varied through the period of analysis, particularly during the first decades of the series and until the mid-twentieth century. The changes observed, particularly before 1950, are consistent with those described in Smith and Reynolds (2004b; Fig. 5), which did not consider them as representative of the actual variability of the SLP and attributed them to the scarcity of data, the quality of the measurement instruments and the dominance of SLP observations taken aboard sailing ships. In fact, these authors proposed that SLP data in the second half of the nineteenth century is affected to a great extent by the changes in the routes of ships during the transition from sail to motor-vessels, and improvements in the forecasting of severe storms, allowing the ships to avoid low-pressure centres. Finally, the global mean values of the zonal and meridional components of the wind do not show any trend (figure not shown). In fact, it is worth mentioning that derived variables, like pressure gradients, are not significantly affected by the application of this method. We have confirmed that pressure gradients in the North Atlantic domain remain basically unchanged when computed using original 20CR SLP data or its 'internal variability' version. Finally, a comparison has been made between the evolution of the globally averaged values of surface air temperature

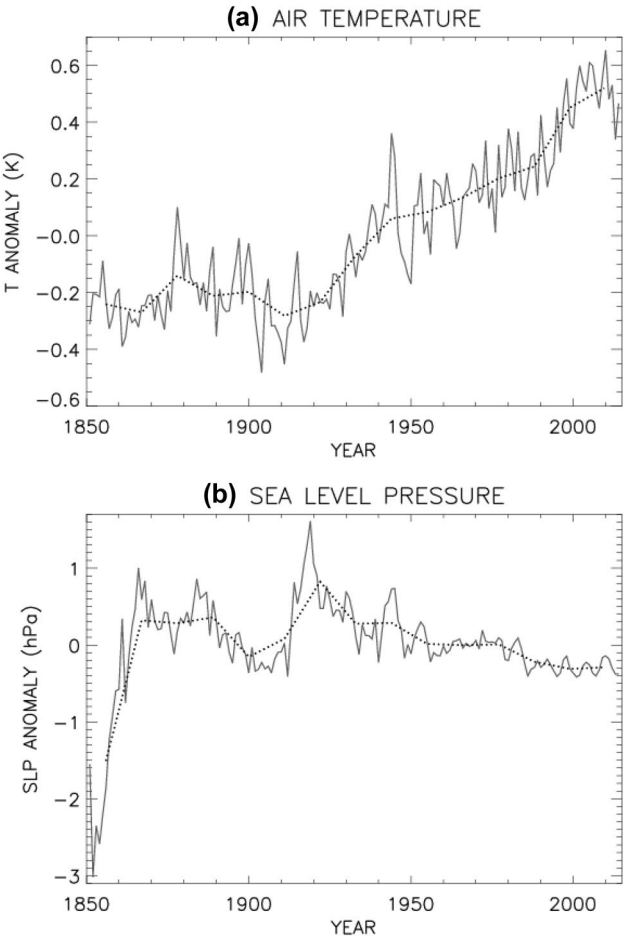

Fig. 1 Annual evolution of **a** global mean air temperature anomalies and **b** global mean SLP anomalies (20CR). Dotted lines represent their 11-year moving average

and SLP obtained from ERA20C with those obtained from 20CR. The result is that both variables show an almost identical evolution during their common period, between 1900 and 2010 (figure not shown). The coincidence in the evolution of both SLP series would seem to reinforce the idea that the origin of the anomalies observed in SLP evolution has to do with the characteristics of the observations rather than with the assimilation models employed to generate the reanalyses.

In addition to these datasets, several climatic indices have been used in this paper. The AMO index has been obtained using the Kaplan SST reanalysis. The index is computed as the annual anomaly of the area weighted average of the SST data within the North Atlantic basin, in the region between 0° to 60° N and between 70° W and 10° E. Then, the method proposed in Ting et al. (2009) is used to separate internal and forced variability. The AMO index has been converted into an annual index by computing the mean annual value of the corresponding monthly anomalies. The final AMO series covers the period from 1856 to the present and has been used to define the evolution in the phase of the multidecadal oscillations detected when the MTM-SVD method (Mann and Park 1999) is applied to the different datasets.

The North Atlantic Oscillation (NAO) represents the main mode of climate variability of the atmosphere in the North Atlantic region, including Western Europe and eastern North America (Hurrell 1995). The NAO index from the Climatic Research Unit repository (University of East Anglia; Jones et al. 1997) has been used to assess the connection between the atmosphere, the ocean circulation and AMO.

The Greenland Blocking Index (GBI: 1851–2015), developed in Hanna et al. (2016), is also utilized in this paper. This index has been included because previous literature proposed that, depending on the position of a blocked regime over the North Atlantic, the associated wind forcing could favour the development of a particular phase of the AMO (Häkkinen et al. 2011). Thus, the GBI can be a good tool to assess this relationship between blocked regimes and AMO.

2.3 Description of the methods

In order to identify and reconstruct the AMO signature in all these multivariate datasets we applied the MTM-SVD methodology as in Delworth and Mann (2000), but explicitly separating the internal and 'forced' signals in each series. The MTM-SVD method identifies and reconstructs narrowband oscillations that are significant in a representative number of series of the original dataset. The method transforms the original series from the time domain to the frequency domain through the use of multitaper spectral analysis. In accordance with convention, three tapers and a time–frequency bandwidth product of w = 2 N, which limits the maximum detectable period to about 80 years, will be used. In the frequency domain, MTM-SVD applies the singular value decomposition method for each representative frequency. The first eigenvalue from each SVD explains the maximum variance for each particular frequency and is termed the local fractional variance (LFV). Plotting LFV values against all the possible frequencies provides an LFV spectrum, which can be used to identify the most significant common oscillations in the original database. A bootstrap method with 1000 random combinations of the original data, with the same spatial structure but with different temporal characteristics, is used to calculate statistical significance levels (90%, 95% and 99% were used here). If a band of frequencies is detected as significant, a representative frequency can be selected to reconstruct the evolution of the spatial pattern associated with that frequency. In addition, the method can be used to reconstruct the time series representing the evolution associated with that frequency at any of the original grid points.

In this paper, the MTM-SVD method will be applied to all the data collections separately, providing an independent analysis for each variable. Then, all the atmospheric variables will be combined into a single database that will be analysed as a whole.

Finally, we assessed possible links between AMO and other climatic modes of variability by the analysis of cross-correlation functions (CCFs) between AMO series and those series representing NAO and GBI. We applied a low pass filter to the NAO and GBI series in order to eliminate high frequency variability in their correlation with AMO. The application of those filters implies that in order to calculate the level of confidence of the CCFs, the degrees of freedom will have to be reduced accordingly. This reduction was carried out in accordance with the procedure described in Oort and Yienger (1996). To obtain stable estimates of the corresponding degrees of freedom, as many lags as needed were permitted in the decorrelation procedure. Even with original series of 161 years, values as low as 20 degrees of freedom have been obtained in some cases including lags of 50 years in the decorrelation procedure.

3 Results

3.1 Separating internal variability and external forcings

Figure 2a shows the LFV spectra obtained from the original SST datasets, which include internal and forced variability. As expected, the four LFV spectra obtained from the different SST reanalyses show very similar characteristics. A wide oscillation band centred in 0.23 cycles per decade was detected at a statistically significant level in the four

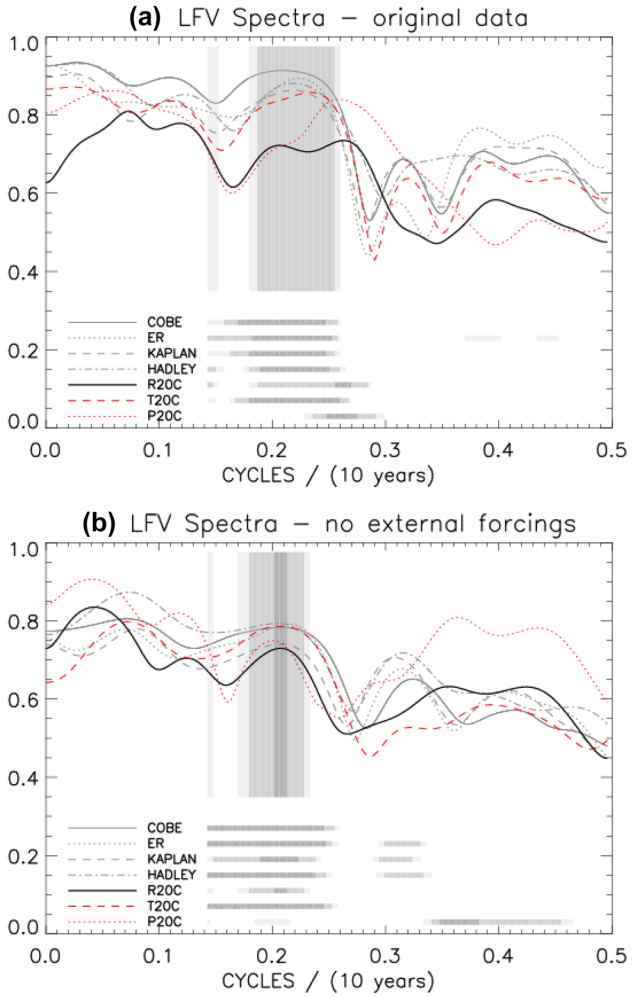

Fig. 2 LFV spectra of **a** the original SST and atmospheric reanalyses (20CR: combined field of SLP, air temperature and zonal and meridional components of the wind; P20C and T20C represent individual fields of SLP and air temperature); and **b** the same datasets but without 'external forcings'. Confidence levels: $p<0.10$ (light grey), $p<0.05$ (grey) and $p<0.01$ (darker grey). Shadowed bands over the LFV spectral lines indicate frequencies where the four SST and the 20CR datasets show those same confidence levels. At the bottom of both panels, information about the confidence levels of LFV spectra for each field and frequency are indicated (same confidence levels as before)

datasets. Some secondary oscillation bands can be observed in the different LFV spectra, but they are not simultaneously significant in all the datasets. The most prominent of those secondary oscillations has frequencies varying between 0.37 and 0.47 cycles per decade (a period ranging between 22 and 27 years).

When external forcings are removed from the original datasets and MTM-SVD is applied to the resulting SST fields, some differences were seen between the new and the previous LFV spectra (Fig. 2b). In this case, all of the databases are characterized by a statistically significant broad oscillatory band centred approximately on 0.21 cycles per decade, slightly less than the one previously obtained. This result is somewhat similar to the one obtained by Trenberth and Shea (2006) when working with a single series of the AMO index. In that paper, it was suggested that the representative period of the AMO is a little longer when external forcings are extracted from the AMO index series. In addition, the most evident secondary band, originally centred on $f=0.40$ cycles per decade, is displaced towards longer periods and a better correspondence is observed among the four new SST datasets.

In an attempt to identify the mechanisms responsible for this multidecadal variability and associated climate impacts, the same procedure was applied to surface air temperature, sea level pressure and meridional and zonal components of surface wind.

As in the previous analysis, the LFV spectrum of the joint original atmospheric datasets, before external forcings were removed, is characterized by a significant broad multidecadal band (thicker line in Fig. 2a). This band is wider than the one obtained from SST datasets and it broadens toward higher frequencies. When air temperature and SLP are analysed separately (red lines), it becomes evident that SLP is responsible for the higher frequency peak (0.26 cycles per decade) in the LFV spectrum of the combined dataset and, as a consequence, for the differences observed between the LFV spectra of the oceanic and atmospheric datasets. LFV spectra obtained for air temperature and SLP from ERA20C show characteristics very similar to those observed with the 20CR data. In both cases, SLP is characterized by a multidecadal band with a higher frequency ($f=0.28$ cycles per decade) than that of the air temperature ($f=0.26$ cycles per decade). The main difference between the multidecadal oscillatory bands obtained for ERA20C and those obtained for 20CR is that the ERA20C bands are displaced towards shorter oscillation periods, probably due to the shorter duration of the available data (figure not shown).

The LFV spectra obtained from atmospheric data after the external forcings were removed (Fig. 2b) show some interesting differences in comparison with the LFV spectra of the original atmospheric datasets before the external forcings were removed (Fig. 2a). The multidecadal bands obtained from the atmospheric and oceanic datasets show much greater similarities among them than they exhibited before the external forcings were removed, showing an almost identical central peak in all cases. In addition, when air temperature and SLP are independently analysed, the most intense peaks in their respective LFV spectra are almost coincident. In this case, however, the 20–30-years period has almost disappeared from the temperature spectrum while it has gained importance in the SLP spectrum. The remarkable coincidence in the main AMO oscillatory band observed ($f=0.208$ cycles per decade) in the spectral

characteristics of the SLP and air temperature fields when external forcings are removed supports the idea that this multidecadal oscillation is an internal climatic signal with a notable impact over all these fields. In fact, the LFV spectra of the original datasets show that the impact of this internal signal over both variables is notably distorted when external forcings are not removed. Similar results are obtained when air temperature and SLP from ERA20C are analysed. As occurred with the LFV spectra for 20CR data, the new central frequencies for ERA20C air temperature and SLP data, once external forcings are removed, are almost identical. In addition, the main oscillatory band for both variables without external forcings peaks at a lower frequency (f = 0.22 cycles per decade) than with the raw data (figure not shown).

To check if the detected oscillatory bands are representative of AMO, the corresponding reconstructed principal components were calculated using the highest peak in the most intense oscillatory band identified with the LFV spectra. A frequency of f = 0.220 cycles per decade was used for the original reanalysis data, while f = 0.208 cycles per decade was used for the series without external forcings. Figure 3a shows the original AMO series, linearly detrended, and the reconstructed principal component series using the original SST and 20CR datasets. Figure 3b shows the corresponding AMO series without external forcings and the corresponding reconstructions obtained from the fields without external forcings. It is evident that the original AMO series and the reconstructed series are very similar in both cases. Pearson correlation coefficients between the original series and the reconstructions range from r = 0.65 to r = 0.68 (P < 0.01). These coefficients are slightly lower when the reconstructed series are obtained from datasets without external forcings, with values ranging from r = 0.53 to r = 0.58 (P < 0.01). A previous study (Trenberth and Shea 2006) found that the amplitude of the index oscillation is reduced when external forcings are removed from the data, in a similar way to what we observed in Fig. 3. In addition, it is interesting to note that when the high frequency variability of the original AMO series is eliminated by applying, for example, a moving window of 9 or 11 years, the correlation coefficients reach values of r = 0.9, both when series are reconstructed from the original datasets and when external forcings have been removed from those datasets. These results suggest that long period multidecadal oscillations are well captured by the corresponding oscillatory band detected by the LFV spectra and that they are representative of the AMO multidecadal variability. However, higher frequencies, representing interannual variability, are not so well captured in these reconstructions.

Figure 4 shows two sets of evolutive LFV spectra using a moving window of 135 years. Figure 4a and c, show LFV spectra of the data before external forcings were removed, while Fig. 4b and d, show the spectra after external forcings

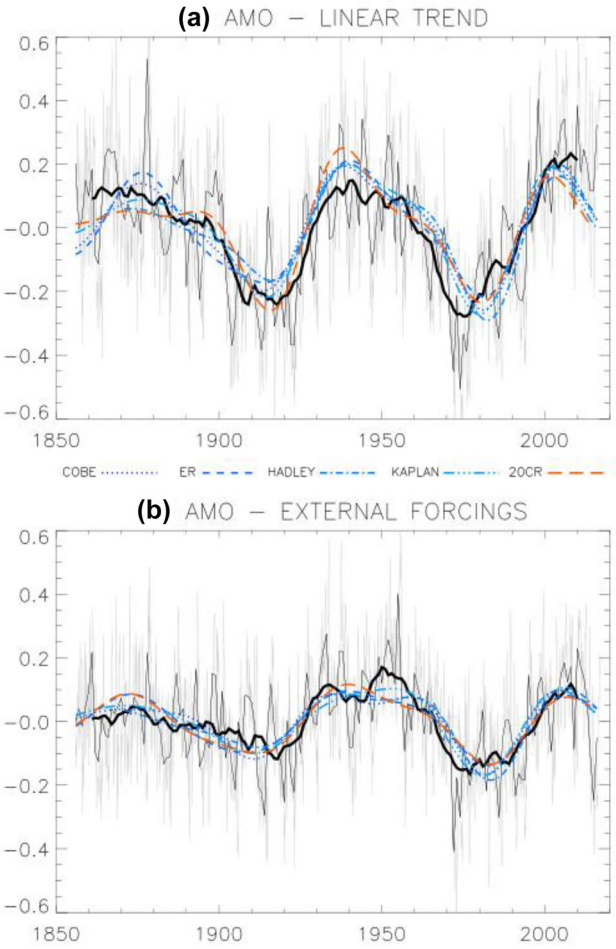

Fig. 3 AMO original and reconstructed (from the central peaks observed in the different LFV spectra) series (light grey: monthly; grey: annual; thick black: 11-year moving average of the annual data). The series obtained from the SST data is in blue, and the series from the combined 20CR datasets is in red. **a** Shows the series obtained from the original series and **b** those obtained from the series without 'external forcings'

were removed. Figure 4a and b, show LFV spectra of oceanic variables, while Fig. 4c and d, show atmospheric variables. ER-SST data has been used to show the evolutive spectra representing the oceanic variability but results from other reanalyses are quite similar to those presented here (not shown). It is interesting to note the differences between these evolutive spectra before and after removing the external forcings from the original datasets. The spectrum of the original SST field shows an evolution in its main oscillatory band; its most prominent frequency peak varies between the early and late years of the analysed period, from a central frequency slightly higher than 0.20 cycles per decade in the early decades to a central frequency of about 0.24 cycles per decade in the most recent years. This evolution could be interpreted as representative of a variation of the main oscillatory period of the AMO. However, this characteristic

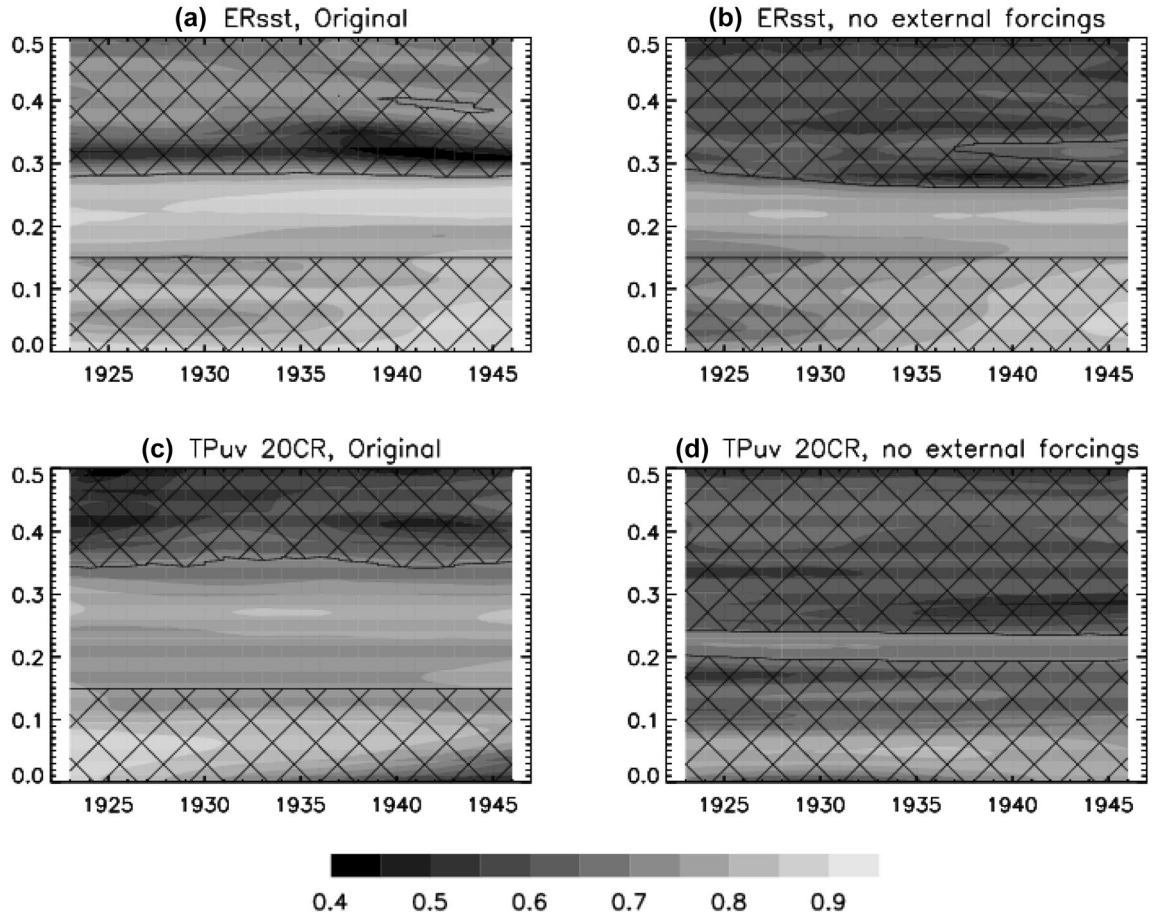

Fig. 4 Evolutive LFV spectra with a 135-year window obtained from ER-SST (**a** and **b**) and from the combined 20CR datasets (**c** and **d**); from the original reanalyses (**a** and **c**) and from the datasets without external forcings (**b** and **d**). Y-axis: frequency; X-axis: central year of the analyzed period. Non-significant frequencies and years crossed out with crossed lines ($p < 0.1$)

is no longer seen in the evolutive spectra of the SST data when the external forcings have been removed. In fact, the evolutive LFV spectra of SST data without external forcings show a period almost constant over time. This indicates that the characteristic oscillatory period of AMO remains stable through the period of analysis, as would be expected if the AMO is an essentially internal signal of the climatic system. These differences between the results obtained before and after external forcings were removed are not so evident in the evolutive LFV spectra of the atmospheric variables. But it is interesting to note the existence of a very stable main oscillatory period in the evolutive LFV spectrum obtained from the atmospheric data with the external forcings removed. In fact, this main oscillatory band is very similar to the one obtained from SST without external forcings, with a central frequency of approximately 0.208 cycles per decade.

The reconstruction of the evolution of the SST over the North Atlantic ocean through half an AMO cycle using a frequency of $f = 0.208$ cycles per decade is presented in Fig. 5, while the evolution of the corresponding patterns for the atmospheric variables over the same time period is shown in Fig. 6. These reconstructions were made using the original datasets (left column in both figures) and the datasets in which the external forcings have been removed (right column in both figures). These figures show the evolution of the spatial patterns through consecutive phases of the AMO cycle, beginning at phase 0° (maximum positive value of the AMO index: first row—subfigures a and b in Figs. 5 and 6) and ending at phase 150° (20 years later: last row in both figures—subfigures k and l). Phases are shown every 30° (a timestep of approximately 4 years). Oceanic results are only shown for ER SST, but those obtained for the other datasets were very similar (not shown).

As expected, the characteristics of the spatial pattern of SST in phase 0° is very similar to the classic AMO pattern, with warmer than normal conditions over the North Atlantic basin. In this case, the most notable difference between the patterns obtained from data with (Fig. 5a) or without (Fig. 5b) external forcings is found in the intensity of the anomalies, with warmer conditions in Fig. 5a (raw data).

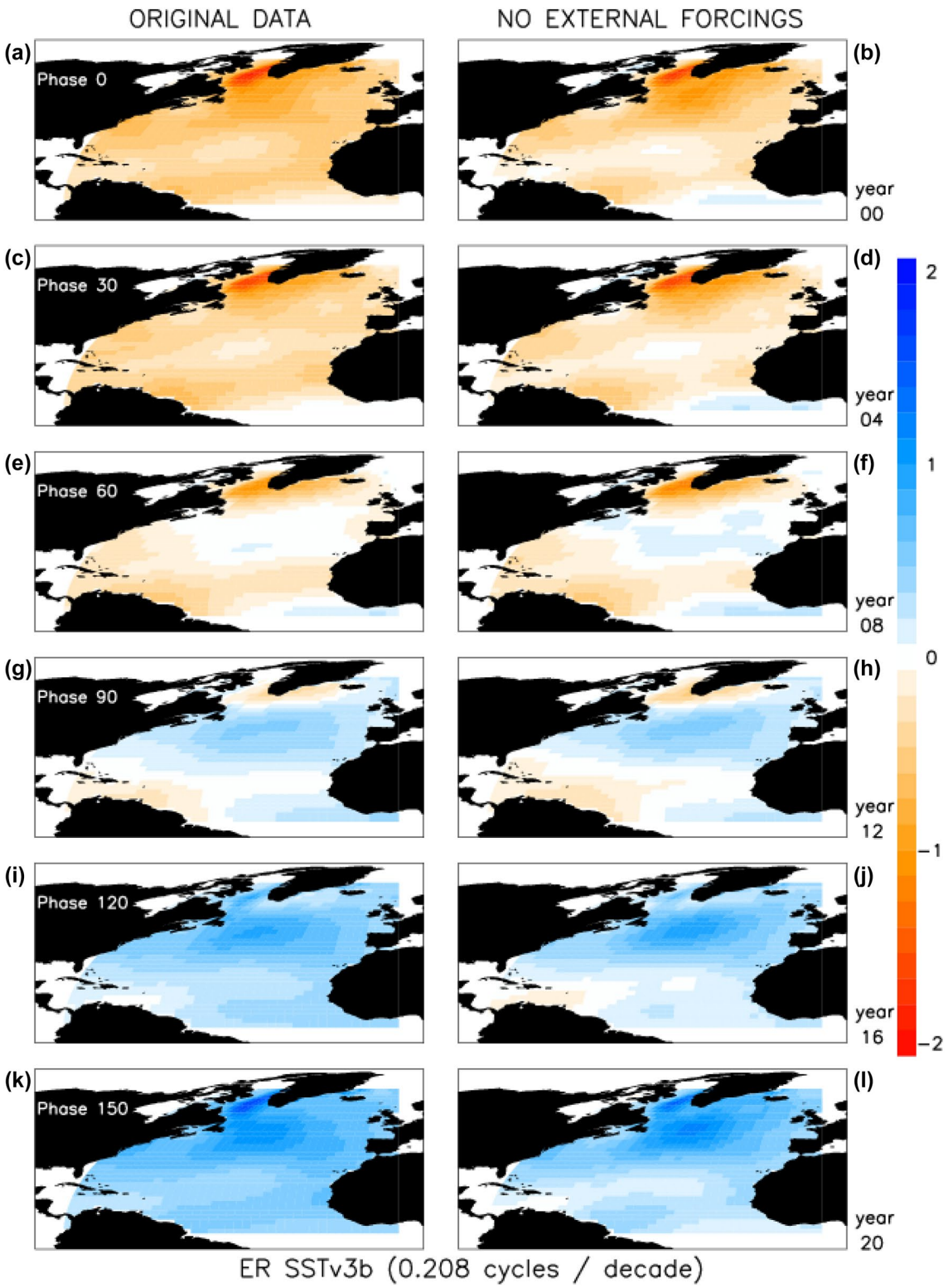

Fig. 5 Reconstruction of the evolution of original ER-SST (left column) and ER-SST without external forcings (right column) throughout half an AMO cycle using f = 0.208 cycles per decade. The maps in the row above correspond to phase 0° of the oscillation (AMO maximum, year 0). The following phases correspond to successive phase shifts of 30° (Phases are included within the maps in the left column and correspond to time-steps of 4 years). Color scale: temperature anomalies (Celsius)

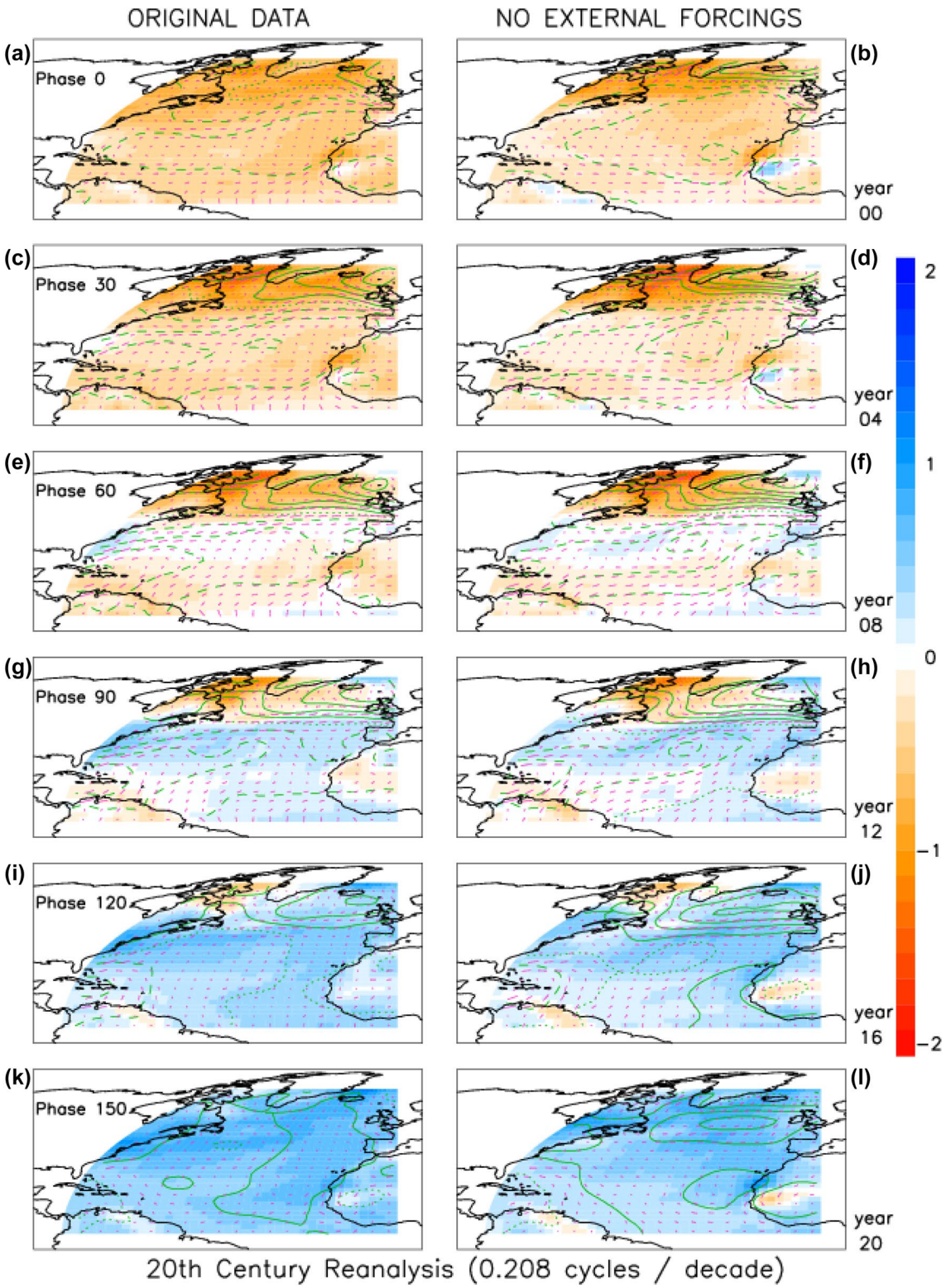

Fig. 6 Reconstruction of the evolution of air temperature, SLP and wind anomalies obtained from the original data (left column) and from the data without external forcings (right column) throughout half an AMO cycle using f = 0.208 cycles peer decade. The maps in the row above correspond to phase 0° of the oscillation (AMO maximum, year 0). The following phases correspond to successive phase shifts of 30° (Phases are included within the maps in the left column and correspond to time-steps of 4 years). Color scale: temperature anomalies (Celsius). Continuous (discontinuous) line contours represent positive (negative) SLP anomalies. Small magenta arrows represent the wind, the length of the arrow is proportional to intensity at each point

Figure 5b shows that most of the North Atlantic Ocean is warmer than normal, particularly around the Labrador Sea, and only a small area of slightly cold anomalies can be observed west of the Gulf of Guinea. This area of slightly cold anomalies is not seen in Fig. 5a. In fact, comparing Fig. 5a and b, shows that differences in the intensity of SST anomalies are more evident in the tropical and subtropical areas. Atmospheric temperature at the surface (Fig. 6a and b) shows basically the same patterns as those of SST. The whole basin is characterized by warmer than normal conditions, but there are small areas with positive anomalies at low latitudes in Fig. 6b that are not seen in Fig. 6a. On the other hand, sea level pressure in Fig. 6b is characterized by a dipolar structure, with higher than normal pressure over Iceland and extending toward Greenland, and lower than normal pressure over the southern North Atlantic, near about 25° N. This dipole resembles the negative phase of the NAO but with the centre of its subtropical pole displaced southward. This dipolar structure is not so evident or so intense in the SLP pattern obtained from the raw data (Fig. 6a). In this case, there is a zonal band of negative anomalies crossing the Atlantic Ocean between the Caribbean Sea and Northern Africa/Southern Europe; but the centre of positive anomalies over Iceland observed in Fig. 6b is not so well developed or so intense in Fig. 6a.

Four years later, in phase 30° (second row in Figs. 5 and 6), the observed patterns are similar to those in phase 0°. Positive anomalies cover most of the area, both for SST and air temperature, but this time their values are slightly lower than in the previous phase. The most noticeable difference between phases 0° and 30° is observed in the pattern of SLP. In Fig. 6d, the previously described dipolar structure remains but the meridional gradient has become more intense and its similarity with the negative phase of NAO is more evident, with the central sector of the negative anomalies located between the Azores and Bermuda. On the other hand, Fig. 6c shows a much better developed centre of high-pressure anomalies over Iceland, but the centre of the low-pressure anomalies is clearly displaced toward the United States, and so in this respect not similar to the NAO dipole.

In the following years, during phases 60° and 90° (8 and 12 years respectively after the maximum in the AMO index; 3rd and 4th rows in Figs. 5 and 6), the signs of SST and air temperature anomalies begin to change for both original data and data without external forcings. These changes are most evident in the central band of the ocean, from the coast of the US to southern Europe and northern Africa, in the lowest analysed latitudes and in a small region in the northeast corner of the map, to the east of Iceland (Figs. 5f and 6f). Later, in phase 90°, the eastern half of the southern North Atlantic cools and its temperature is characterized by negative anomalies. Again, it is interesting to note the evolution of the SLP. Both in the original data patterns and in the 'no external forcings' patterns, anticyclonic anomalies remain intense over Iceland and increase their influence toward the west and the south. On the other side, cyclonic anomalies in Fig. 6f and h, are not so intense and their area of coverage is reduced, with an apparent retreat toward the Gulf of Mexico. The similarities between the SLP anomalies during these two phases and the pattern of a negative NAO can still be seen. In Fig. 6e and g, the situation evolves in a similar way except that the centre of the cyclonic anomalies is much closer to the US coast than it is in Fig. 6f and h and the SLP dipole does not have a meridional character but rather shows a SW-NE direction.

Phase 120° (16 years after the AMO maximum: 5th row in Figs. 5 and 6) is characterized by a generalized oceanic and atmospheric cooling. Only small areas of positive temperature anomalies are seen in all cases except for Fig. 5i (pattern for SST raw data). The greatest positive anomaly is observed in air temperature over Baffin Bay and Labrador. By this time-step the NAO-like structure and the diagonal SLP gradient have disappeared and higher than normal pressures are observable over most of the North Atlantic basin, particularly in the pattern obtained for SLP without external forcings (Fig. 6j). But what is more interesting is that an intense blocking-like anticyclonic circulation covers a large area that includes Greenland, Iceland and the British Isles. These SLP positive anomalies are not so intense in the case of the pattern obtained from the raw data (Fig. 6i). Phase 150°, four years before an AMO minimum, is very similar to phase 120°. By phase 150°, the patterns for data with no external forcings are characterized by negative temperature anomalies over the entire Atlantic Ocean, while positive SLP anomalies cover the entire area except for a small region in the Caribbean Sea. And, again, a centre of positive SLP anomalies is still seen between Greenland and the British Isles, though not so intense or extensive as four years before (Figs. 5l and 6l). These descriptions could be applied to the patterns for the raw data except that the temperature anomalies are more intense and the SLP anomalies are somewhat lower, with a much more disperse distribution, and with no clear centres of action (Figs. 5k and 6k).

Finally, comparing the evolutions of the reconstructed spatial patterns of the SLP fields before and after external forcings were removed yields an interesting result: differences among these patterns are more evident in the middle and low latitudes. This result is in agreement with some previous publications which found that, at decadal scales, the impact of the external forcings on the evolution of temperature was much stronger at low latitudes than at higher latitudes, particularly over the North Atlantic (Ting et al. 2009; Hurrell et al. 2004). In this case, it can be seen that this impact is observable not only in the evolution of temperature, but in the evolution of SLP.

3.2 Ocean–atmosphere interactions

The joint evolution of the oceanic and atmospheric patterns shown in Figs. 5 and 6, especially when external forcings were removed from the data, suggests a constant interaction between these two systems. Changes in AMO phases, characterized by anomalies in the North Atlantic SST, could be caused by changes in the persistence or the intensity of a particular phase of the NAO, or in the frequency, intensity or persistence of blockings over the northern North Atlantic. Furthermore, it is plausible to think that the evolution of the SST anomalies is the cause of the variations in the persistence of a particular phase of NAO or in the frequency and intensity of blockings over the area. We assessed the dynamic connection between the ocean and the atmosphere further using a statistical approximation. Figure 7 shows the cross-correlation functions between the winter GBI and winter NAO series, smoothed by the application of a low-pass filter, and the original AMO series without external forcings together with the AMO reconstructed series obtained after applying the MTM-SVD to the ER SST dataset. This reconstructed series should be interpreted as similar to the ones smoothed by the application of a low-pass filter, which justifies the higher values obtained for the correlations and the differences in their confidence limits. Series reconstructed from the other datasets produce results very similar to those presented for ER SST.

Figure 7a shows the existence of significant positive correlations when the AMO signal precedes the GBI signal. The value of the correlation coefficients is quite high 4–11 years after AMO reaches its maximum, with the highest values of the lagged correlation occurring between lags − 9 and − 6 (when the confidence in their statistical significance is highest as well). There is a good concordance between CCF results using the filtered series and the non-filtered series of AMO but, as expected, the variance is higher with the filtered data. In addition, the lags with the highest correlation coefficients are in very good agreement with the evolution of SLP patterns shown in Fig. 6, where maximum SLP positive anomalies over Greenland are reached at phase 60°, 8 years after the AMO maximum. Thus, there seems to be a connection between AMO and Greenland blockings, with the positive phase of the AMO leading to more frequent and persistent blocking episodes. This result supports the scheme proposed by Hakkinen et al. (2011), who suggest that the occurrence of persistent blockings over the northern North Atlantic, between Greenland and Western Europe, coincide with a warmer North Atlantic Ocean. Further correspondence between results in Figs. 6 and 7 can be seen in the observation that the GBI and AMO series reach their highest correlations between 1 and 12 years after an AMO maximum (more intensely between lags − 11 and − 4) (Fig. 7a). By those years, Fig. 6d, f and h, show the most intense positive SLP anomalies between

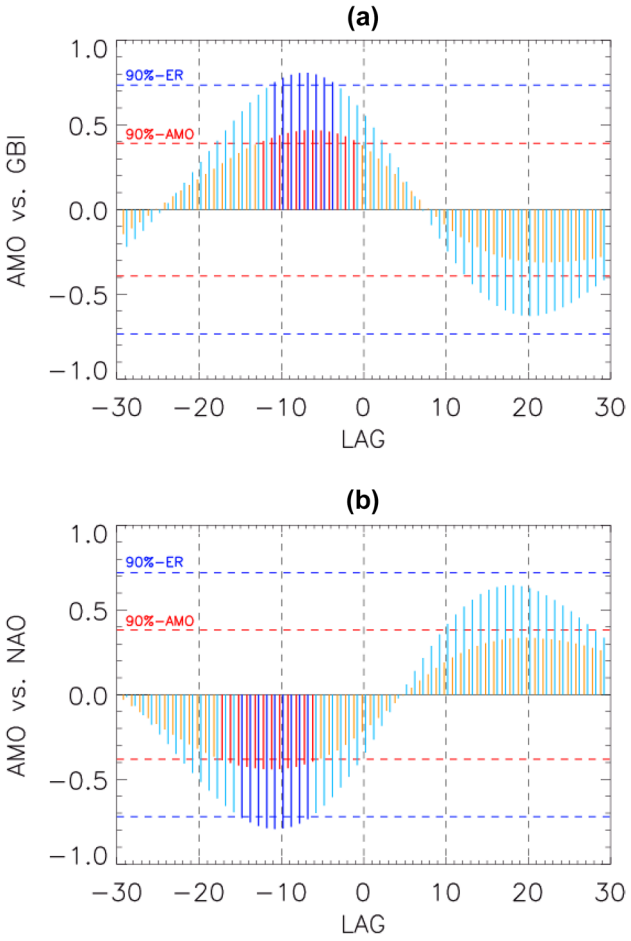

Fig. 7 Cross Correlation Functions between two AMO series (reddish bars: annual AMO index without external forcings; blueish bars: AMO reconstructed index obtained by reversing the MTM-SVD procedure with f = 0.208 cycles per decade, using ERsst data without external forcings) and low-pass filtered series of **a** GBI and **b** NAO. Negative (positive) lags denote that AMO precedes (follows) winter GBI (**a**) or winter NAO (**b**) (level of confidence: 90%, darker and thicker bars). The number of degrees of freedom used to determine confidence levels were computed following Oort and Yienger (1996)

Greenland and Western Europe. Due to the oscillatory character of our reconstruction and the spatial patterns associated with the evolution of AMO, the highest occurrence of blockings between phases 30° and 90° (4–12 years after an AMO maximum) precedes an AMO minimum (AMO negative phase) by 20–12 years. This behaviour is shown in Fig. 7a, in which the maximum negative lagged correlation between the two indices is reached when GBI precedes AMO by about 20 years. But those lagged correlations do not reach a value of $p < 0.1$. These results suggest that it is the ocean which leads the coupled ocean–atmosphere variability, but even when atmospheric conditions seem to exert some impact over the evolution of SST, it is not clear that these atmospheric conditions, in this case the persistence (absence) of blockings over

Greenland, lead to a transition towards the negative (positive) phase of the AMO.

The link between AMO and winter NAO is shown in Fig. 7b. As with GBI, the oscillatory character of the CCF between AMO and NAO indices is evident, with significant negative correlations lasting several years when AMO precedes NAO; and positive but not significant correlations when NAO precedes AMO. The highest negative correlation between the two oscillations is obtained about 10 or 11 years after an AMO maximum. These results are in agreement with Peings and Magnusdottir (2014) who found that the AMO signal precedes NAO by 10–15 years. In fact, Fig. 7b shows that the value and, especially, the sign of the lagged correlation between the two indices are quite stable for a much longer period (about 6–17 years). It is also interesting to note the similarities between Fig. 7a and b: the two CCFs are almost mirror images of each other. This result indicates that the frequency and position of blocking episodes over the North Atlantic sector are very closely anti-correlated with the intensity of NAO, as proposed in Hanna et al. (2016) and Yao and Luo (2015). As with GBI, these lags in the maximum correlations between NAO and AMO can be clearly seen in the evolution of the spatial patterns shown in Fig. 6. A spatial pattern that resembles the negative phase of NAO can be observed between years 4 and 16 after an AMO maximum (negative correlation), most evidently in the patterns corresponding to years 8 and 12 (Fig. 6f and h). A direct consequence is that the maximum value of the negative phase of AMO (year 24) is reached about 12–16 years after NAO reaches its minimum value. The evolution of the spatial patterns of SLP shown in Fig. 6 is also in good agreement with the mechanism proposed by Peings and Magnusdottir (2014), who found that SST conditions associated with the evolution of the AMO phase would induce a shift in the atmospheric baroclinic zone, and that this shift would lead to the changes observed in some atmospheric variables (in this case, GBI and NAO). In this regard, it has been proposed that the forcings produced by NAO-induced variability are required to explain the multidecadal oscillations in oceanic variability and thus, NAO would somehow function as an AMO predictor (Mecking et al. 2014; Wills et al. 2019). Our results show that persistent positive correlations between lagged AMO and NAO series are obtained when NAO preceded AMO by at least 5 years, but none of those coefficients reached a 90% statistical confidence. Therefore, we cannot consider NAO as a predictor of AMO. Nor can we be assured that a long-lasting NAO phase leads to the transition of AMO toward a phase of the same sign.

4 Discussion and conclusions

It is generally accepted that reanalysed climatic datasets are among the most reliable collections of observational data when global spatial and long temporal coverages are required. But, like any other long-duration observational datasets, reanalysed datasets include superimposed information about internal processes of the climatic system, external forcings and even systematic biases inherited from the observational data from which these reanalyses are built. The consequence is that when one seeks to analyse the characteristics of an internal process of the climatic system using reanalysed datasets, it is very important to effectively separate the internal climatic variability from any other signals.

In this paper, we adopted a generalized concept of 'external forcings' and applied the method proposed by Ting et al. (2009) to remove any external forcings from the variables included in the analysed datasets. Only after all external forcings were properly removed was an intense coherent multidecadal oscillation observed. This oscillation is characterized by a common period ranging between 40 and 70 years, in all the SST, SLP and air surface temperature fields over the North Atlantic. This signal is, with an evident alignment among the spectral characteristics of all the different datasets, perfectly compatible with the frequencies typically attributed to the AMO. It is worth noting that this fit is not so good when the 'external forcings' are not removed. Especially striking is the case of the SLP and air temperature datasets. Before external forcings were removed, both datasets showed multidecadal variability with a time scale compatible with AMO, but their main oscillatory bands were clearly not equivalent. However, once external forcings are removed, the main oscillatory bands of SLP and air temperature display an almost perfect fit.

In order to check the robustness of these results, a similar analysis was performed with a dataset from shorter reanalysis, ERA20C. This analysis yielded very similar results: a very good fit between the multidecadal oscillation bands obtained for the ERA20C dataset SLP and surface air temperature, when 'external forcings' were removed from the data; and non-coincident frequency peaks for their main multidecadal oscillatory bands when the analysis was performed with the raw data. In addition, it must be stressed that the 40–70-years characteristic period we have found to be consistent among different variables remains constant in time only when the external forcings are removed. This constant character of the oscillatory period is what is expected for an oscillation resulting from truly internal processes of the climatic system. These results stress the importance of eliminating

the external forcings before characterizing internal climate variability processes for every variable. This is essential even for the SLP, a variable which has traditionally been considered to be unaffected by human activities or almost any other external forcing.

It is interesting to point out the differences in the origins of the 'external forcings' detected in the temperature and SLP datasets. In the previous literature, it has been proposed that long-duration temperature series are affected primarily by changes in the radiative forcing, mainly due to the effect of the increasing concentration of greenhouse gases, but also due to the anthropogenic and natural emission of aerosols (Frankcombe et al. 2015; Mann et al. 2014; Ting et al. 2009; Trenberth and Shea 2006). On the other hand, it is believed that the global mean value of the SLP is not affected by those emissions, since the total mass of the atmosphere remains constant in time. But when the annual evolution of the 20CR SLP global mean value is analysed, a notable and positive trend is detected. That trend is concentrated in the early decades of the series and most probably has its origin in the scarcity of data and in problems in the instruments employed and/or in the recording of the early SLP data (Smith and Reynolds 2004b).

When the spatial characteristics of our reconstructions are used to analyse the relationship between the ocean and the atmosphere, evidence of a cyclic behaviour is observed: Initially, when the AMO reaches its maximum positive phase, the ocean seems to enhance the occurrence of blocking events between Greenland and the west coast of Europe, which, it has been proposed, favours the persistence of warm anomalies in the northern North Atlantic (Häkkinen et al. 2011). After a few years, a negative NAO-like pattern develops, as proposed in Peings and Magnusdottir (2014). This pattern persists for several years and leads to a cooling of the ocean surface, which in turn leads to a negative phase of AMO which, when it reaches its minimum, favours a lower frequency of blockings over Greenland. A few years later, the development of a positive NAO-like pattern leads to the next positive phase of AMO.

The problem with this mechanism arises when analysing the lagged correlations observed in the CCFs between the different climatic indices representing AMO, blockings over Greenland and NAO. The analysis of these CCFs, which is in good agreement with the evolution of our reconstructed spatial patterns, shows that during the decade following an AMO maximum (minimum), blockings over Greenland become more (less) frequent. A similar interpretation is obtained when the connection between AMO and NAO is analysed, also yielding a significant correlation, but of the opposite sign. Thus, positive AMO values precede negative NAO phases. On the other hand, our analysis of the CCFs does not support the view that the persistence of NAO in one phase (or a higher frequency of blockings over Greenland) leads to a transition in the phase of AMO. In other words, our results provide evidence for the view proposed by Gulev et al. (2013), in the sense that, at multidecadal time-scales, the ocean is the system inducing changes in atmospheric conditions, such as the frequency of blocking episodes or the persistence of NAO in a particular phase. But from a statistical point of view, at least, the atmospheric conditions over the ocean do not appear to show such a direct impact.

Acknowledgements This research was funded by the research group RNM-356 belonging to the "Plan Andaluz de Investigación Desarrollo e Innovación (PAIDI)". SST data provided by the NOAA/OAR/ESRL PSD, Boulder, Colorado, USA, from their Web site at https://www.esrl.noaa.gov/psd/. Support for the Twentieth Century Reanalysis Project dataset is provided by the U.S. Department of Energy, Office of Science Innovative and Novel Computational Impact on Theory and Experiment (DOE INCITE) program, and Office of Biological and Environmental Research (BER), and by the National Oceanic and Atmospheric Administration Climate Program Office.

References

Compo GP, Whitaker JS, Sardeshmukh PD (2006) Feasibility of a 100 year reanalysis using only surface pressure data. Bull Am Meteorol Soc 87:175–190. https://doi.org/10.1175/BAMS-87-2-175

Compo GP, Whitaker JS, Sardeshmukh PD, Matsui N, Allan RJ, Yin X, Gleason BE, Vose RS, Rutledge G, Bessemoulin P, Brönnimann S, Brunet M, Crouthamel RI, Grant AN, Groisman PY, Jones PD, Kruk M, Kruger AC, Marshall GJ, Maugeri M, Mok HY, Nordli Ø, Ross TF, Trigo RM, Wang XL, Woodruff SD, Worley SJ (2011) The twentieth century reanalysis project. Q J R Meteorol Soc 137:1–28. https://doi.org/10.1002/qj.776

Delworth T, Mann ME (2000) Observed and simulated multidecadal variability in the Northern Hemisphere. Clim Dyn 16:661. https://doi.org/10.1007/s003820000075

Deser C, Blackmon M (1993) Surface climate variations over the North Atlantic Ocean during winter: 1900–1989. J Clim 6:1743–1753

Dijkstra HE, Saenz JA, Hogg AM (2014) Energetics of multidecadal Atlantic ocean variability. J Clim 27:7874–7889. https://doi.org/10.1175/JCLI-D-12-00801.1

Folland CK, Parker DE, Kates FE (1984) Worldwide marine temperature fluctuations 1856–1981. Nature 310:670–673

Folland CK, Palmer TN, Parker DE (1986) Sahel rainfall and worldwide sea temperatures. Nature 320:602–606

Frankcombe LM, von der Heydt A, Dijkstra H (2010) North Atlantic multidecadal climate variability: an investigation of dominant time scales and processes. J Clim 23:3626–3638. https://doi.org/10.1175/2010JCLI3471.1

Frankcombe LM, England MH, Mann ME, Steinman BA (2015) Separating internal variability from the externally forced climate response. J. Clim 28:8184–8202. https://doi.org/10.1175/jcli-d-15-0069.1

Gulev SK, Latif M, Keenlyside N, Park W, Koltermann KP (2013) North Atlantic Ocean control on surface heat flux on multidecadal timescales. Nature. https://doi.org/10.1038/nature12268

Häkkinen S, Rhines PB, Worthen DL (2011) Atmospheric blocking and Atlantic multidecadal ocean variability. Science 334(6056):655–659. https://doi.org/10.1126/science.1205683

Hanna E, Cropper TE, Hall RJ, Cappelen J (2016) Greenland Blocking Index 1851–2015: a regional climate change signal. Int J Climatol 36:4847–4861. https://doi.org/10.1002/joc.4673

Hirahara S, Ishii M, Fukuda Y (2014) Centennial-scale sea surface temperature analysis and its uncertainty. J Clim 27:57–75. https://doi.org/10.1175/JCLI-D-12-00837.1

Hurrell JW (1995) Decadal trends in the North Atlantic oscillation and relationships to regional temperature and precipitation. Science 269:676–679. https://doi.org/10.1126/science.269.5224.676

Hurrell JW, Hoerling M, Phillips A, Xu T (2004) Twentieth century North Atlantic climate change Part I: assessing determinism. Clim Dyn 23:371–389. https://doi.org/10.1007/s00382-004-0432-y

Ishii M, Shouji A, Sugimoto S, Matsumoto T (2005) Objective analyses of sea-surface temperature and marine meteorological variables for the 20th century using ICOADS and the Kobe collection. Int J Climatol 25:865–879. https://doi.org/10.1002/joc.1169

Jamet Q, Huck T, Arzel O, Campin JM, de Verdière AC (2016) Oceanic control of multidecadal variability in an idealized coupled GCM. Clim Dyn 46:3079. https://doi.org/10.1007/s00382-015-2754-3

Jones PD, Jónsson T, Wheeler D (1997) Extension to the North Atlantic Oscillation using early instrumental pressure observations from Gibraltar and South-West Iceland. Int J Climatol 17:1433–1450

Kaplan A, Cane M, Kushnir Y, Clement A, Blumenthal M, Rajagopalan B (1998) Analyses of global sea surface temperature 1856–1991. J Geophys Res 103:18567–18589

Kerr RA (2000) A North Atlantic climate pacemaker for the centuries. Science 288(5473):1984–1985. https://doi.org/10.1126/science.288.5473.1984

Knight JR, Allan RJ, Folland CK, Vellinga M, Mann ME (2005) A signature of persistent natural termohaline circulation cycles in observed climate. Geophys Res Lett 32:L20708. https://doi.org/10.1029/2005GL024233

Kushnir Y (1994) Interdecadal variations in North Atlantic sea surface temperature and associated atmospheric conditions. J Clim 7:141–157

Li J, Sun C, Jin FF (2013) NAO implicated as a predictor of Northern Hemisphere mean temperature multidecadal variability. Geophys Res Lett 40:5497–5502. https://doi.org/10.1002/2013GL057877

Mann ME, Emanuel KA (2006) Atlantic hurricane trends linked to climate change. Eos Trans AGU 87(24):233–241. https://doi.org/10.1029/2006EO240001

Mann ME, Park J (1999) Oscillatory spatiotemporal signal detection in climate studies: a multiple-taper spectral domain approach. Adv Geophys 41:1–131

Mann ME, Park J, Bradley RS (1995) Global interdecadal and century-scale oscillations during the last five centuries. Nature 378:266–270

Mann ME, Steinman BA, Miller SK (2014) On forced temperature changes, internal variability, and the AMO. Geophys Res Lett 41:3211–3219. https://doi.org/10.1002/2014GL059233

McCarthy GD, Haigh ID, Hirschi JJM, Grist JP, Smeed DA (2015) Ocean impact on decadal Atlantic climate variability revealed by sea-level observations. Nature 521:508–510. https://doi.org/10.1038/nature14491

Mecking JV, Keenlyside NS, Greatbatch RJ (2014) Stochastically-forced multidecadal variability in the North Atlantic: a model study. Clim Dyn 43:271. https://doi.org/10.1007/s00382-013-1930-6

Oort AH, Yienger JJ (1996) Observed interannual variability in the Hadley circulation and its connection to ENSO. J Clim 9:2751–2767

Parker DE, Jones PD, Folland CK, Bevan A (1994) Interdecadal changes of surface temperature since the late nineteenth century. J Geophys Res 99:14373–14399

Peings Y, Magnusdottir G (2014) Forcing of the wintertime atmospheric circulation by the multidecadal fluctuations of the North Atlantic Ocean. Environ Res Lett 9:034018. https://doi.org/10.1088/1748-9326/9/3/034018

Poli P, Hersbach H, Dee DP, Berrisford P, Simmons AJ, Vitart F, Laloyaux P, Tan DGH, Peubey C, Thépaut J-N, Trémolet Y, Hólm EV, Bonavita M, Isaksen L, Fisher M (2016) ERA-20C: an atmospheric reanalysis of the twentieth century. J Clim 29:4083–4097. https://doi.org/10.1175/JCLI-D-15-0556.1

Rayner NA, Parker DE, Horton EB, Folland CK, Alexander LV, Rowell DP, Kent EC, Kaplan A (2003) Global analyses of sea surface temperature, sea ice, and night marine air temperature since the late nineteenth century. J Geophys Res 108(D14):4407. https://doi.org/10.1029/2002JD002670

Schlesinger ME, Ramankutty N (1994) An oscillation in the global climate system. Nature 367:723–726

Smith TM, Reynolds RW (2003) Extended reconstruction of global sea surface temps based on COADS 1854–1997. J Clim 16:1495–1510. https://doi.org/10.1175/1520-0442-16.10.1495

Smith TM, Reynolds RW (2004a) Improved Extended Reconstruction of SST (1854–1997). J Clim 17:2466–2477. https://doi.org/10.1175/1520-0442(2004)017%3C2466:IEROS%3E2.0.CO;2

Smith TM, Reynolds RW (2004b) Reconstruction of monthly mean oceanic sea level pressure based on COADS and station data (1854–1997). J Atmos Ocean Technol 21:1272–1282. https://doi.org/10.1175/1520-0426(2004)021<1272:ROMMOS>2.0.CO;2

Smith TM, Reynolds RW, Peterson TC, Lawrimore J (2008) Improvements to NOAAs historical merged land-ocean temp analysis (1880–2006). J Clim 21:2283–2296. https://doi.org/10.1175/2007JCLI2100.1

Ting MF, Kushnir Y, Seager R, Li CH (2009) Forced and internal twentieth-century SST trends in the North Atlantic. J Clim 22(6):1469–1481. https://doi.org/10.1175/2008JCLI2561.1

Tourre YM, Rajagopalan B, Kushnir Y (1999) Dominant patterns of climate variability in the Atlantic Ocean during the last 136 years. J Clim 12:2285–2299

Trenberth KE, Shea DJ (2006) Atlantic hurricanes and natural variability in 2005. Geophys Res Lett 33:L12704. https://doi.org/10.1029/2006GL026894

Wills RC, Armour KC, Battisti DS, Hartmann DL (2019) Ocean-atmosphere dynamical coupling fundamental to the Atlantic multidecadal oscillation. J Clim 32:251–272. https://doi.org/10.1175/JCLI-D-18-0269.1

Woodruff SD, Diaz HF, Elms JD, Worley SJ (1998) COADS Release 2 data and metadata enhancements for improvements of marine surface flux fields. Phys Chem Earth 23:517–527

Woodruff SD, Worley SJ, Lubker SJ, Ji Z, Freeman JE, Berry DI, Brohan P, Kent EC, Reynolds RW, Smith SR, Wilkinson C (2011) COADS release 2 data and metadata enhancements. Int. J. Climatol 31:951–967. https://doi.org/10.1002/joc.2103

Xue Y, Smith TM, Reynolds RW (2003) Interdecadal changes of 30-year SST normals during 1871–2000. J Clim 16:1601–1612

Yao Y, Luo D (2015) Do European blocking events precede North Atlantic Oscillation events? Adv Atmos Sci 32:1106. https://doi.org/10.1007/s00376-015-4209-5

Publisher's Note Springer Nature remains neutral with regard to jurisdictional claims in published maps and institutional affiliations.